An X-ray Crystallographic and Single-Crystal EPR Investigation of the Cationic, Iron-Centered Radical Tricarbonylbis(triphenylphosphine)iron(I), $\{Fe(CO)_3(PPh_3)_2^+\}$. A Theoretical Examination of the Structural Preferences of Five-Coordinated Seventeen-Electron Complexes

Joseph H. MacNeil,[†] Antony C. Chiverton,[†] Suzanne Fortier,*[,†] Michael C. Baird,*[,†] Rosemary C. Hynes,[‡] Antony J. Williams,[‡] Keith F. Preston,*[,‡] and Tom Ziegler*[,§]

Contribution from the Department of Chemistry, Queen's University, Kingston, Canada K7L 3N6, The Steacie Institute for Molecular Sciences, National Research Council of Canada,[∥] Ottawa, Canada K1A OR9, and Department of Chemistry, University of Calgary, Calgary, Canada T2N 1N4. *Received April 15, 1991*

Abstract: The X-ray crystal structure of the 17-electron complex $[Fe(CO)_3(PPh_3)_2][PF_6]\cdot{}^1/_2CH_2Cl_2$ has been determined; the compound crystallizes in the space group $P\bar{1}$, and the cation assumes essentially a distorted square-pyramidal structure with trans basal phosphines, a P–Fe–P bond angle of 163.4 (1)°, a (basal CO)–Fe–(basal CO) bond angle of 162.0 (6)°, and (axial CO)–Fe–(basal CO) bond angles of 101.4 (6)° and 96.6 (5)°. The EPR spectrum of the cation $\{Fe(CO)_3(PPh_3)_2^+\}$ has been measured in single crystals of $[Co(CO)_3(PPh_3)_2][PF_6]\cdot CH_2Cl_2$ at 77 K, the **g** and ^{31}P hyperfine interaction matrices being established in an orthogonal axis system of the monoclinic host. X-ray diffraction was used to determine the host crystal structure (space group $P2_1/n$) and to establish the geometry of the diamagnetic cobalt cation as trigonal bipyramidal with axial phosphines (P–Co–P bond angle 176.5 (1)°) and equatorial carbonyl groups (OC–Co–CO bond angles 117.8 (4)°, 119.5 (4)°, and 122.7 (5)°). The radical $\{Fe(CO)_3(PPh_3)_2^+\}$ has a $^2A_1$ ground state, **g** (2.0091, 2.0898, 2.0795) being nearly axial with a unique component that lies almost in the equatorial plane of the host cation and having a value close to that of a free spin. The two ^{31}P hyperfine interaction tensors are coparallel and axially symmetric with unique components directed along the host P–Co bonds. The similarity of the principal values of **g** to those of $\{Fe(CO)_5^+\}$ and their disposition with respect to the host cation show beyond any reasonable doubt that $\{Fe(CO)_3(PPh_3)_2^+\}$ has a geometry approaching square pyramidal, as in crystalline $[Fe(CO)_3(PPh_3)_2]PF_6\cdot{}^1/_2CH_2Cl_2$, and a $^2A_1$ ground state (in C_{2v} symmetry) with the unpaired electron principally located in the iron $3d_{z^2}$ orbital. The phosphine ligands, axial in the host cation structure, occupy trans equatorial positions in the square-pyramidal structure of the cation radical. LCAO-HFS calculations for $\{M(CO)_3L_2\}$ (M = Mn, Fe^+; L = CO, PH_3) are consistent with the finding that $\{Fe(CO)_3(PPh_3)_2^+\}$ assumes a square-pyramidal (C_{2v}) structure and a $^2A_1$ ground state rather than a trigonal-pyramidal (D_{3h}) structure; other bipyramidal isomers are proximate in energy, but have not been observed.

Introduction

The chemistry of 17-electron, metal-centered organometallic compounds has recently become the focus of growing attention, as such radical species are increasingly being recognized as intermediates in a variety of novel chemical reactions.[1] The chemical and electronic structures of 17-electron complexes are also of much interest, but the high reactivities and short lifetimes of most metal-centered radicals have severely limited X-ray crystallogragphic or definitive EPR investigations involving single crystals.[2] As an exception to this general observation, the families of compounds $\{V(CO)_5L\}$[3] and $\{\eta^5\text{-}C_5R_5Cr(CO)_2L\}$ (R = H, Me; L = CO, tertiary phosphines)[4] have been extensively investigated in this manner.

A third family of 17-electron complexes which is proving increasingly amenable to detailed study is comprised of the three five-coordinated, isoelectronic series $\{M(CO)_5^-\}$ (M = Cr, Mo, W), $\{M(CO)_{5-n}L_n\}$ (M = Mn, Re; L = CO, tertiary phosphine; n = 0, 1, 2), and $\{M(CO)_{5-n}L_n^+\}$ (M = Fe, Os). On the basis of a number of investigations involving several spectroscopic techniques, the anionic species $\{M(CO)_5^-\}$,[5] the neutral species $\{Mn(CO)_5\}$[6] and $\{Re(CO)_5\}$,[7] and the cationic iron and osmium species $\{M(CO)_5^+\}$[8] are all believed to assume square-pyramidal (C_{4v}) structures in which the odd electron resides in an essentially d_{z^2} orbital.[9] Tertiary phosphine substituted derivatives of the type $\{M(CO)_3L_2\}$ (M = Mn, Re) are believed to assume similar structures,[10] with trans basal phosphines, an hypothesis confirmed crystallographically in one case at least by the X-ray structure determination of $\{Re(CO)_3(PCy_3)_2\}$.[11]

In contrast, the substituted derivatives $\{Fe(CO)_3L_2^+\}$ are believed on the basis of IR and SCF-Xα-DV calculations to assume

[†] Queen's University.
[‡] The Steacie Institute for Molecular Sciences.
[§] University of Calgary.
[∥] NRCC No. 33255.

(1) (a) Kochi, J. K. *Organometallic Mechanisms and Catalysis*; Academic Press: New York, 1978. (b) Baird, M. C. *Chem. Rev.* **1988**, *88*, 1217. (c) Trogler, W. C., Ed. *Organometallic Radical Processes*; Elsevier: New York, 1989.
(2) Baird, M. C. In *Organometallic Radical Processes*; Trogler, W. C., Ed.; Elsevier: New York, 1989; Chapter 2.
(3) (a) Bellard, S.; Rubinson, K. A.; Sheldrick, G. M. *Acta Crystallogr.* **1979**, *B35*, 271. (b) Boyer, M. P.; LePage, Y.; Morton, J. R.; Preston, K. F.; Vuolle, M. J. *Can. J. Spectrosc.* **1981**, *26*, 181. (c) Bratt, S. W.; Kassyk, A.; Perutz, R. N.; Symons, M. C. R. *J. Am. Chem. Soc.* **1982**, *104*, 490. (d) Holland, G. F.; Manning, M. C.; Ellis, D. E.; Trogler, W. C. *J. Am. Chem. Soc.* **1983**, *105*, 2308. (e) McCall, J. M.; Morton, J. R.; Preston, K. F. *J. Magn. Reson.* **1985**, *64*, 414. (f) McCall, J. M.; Morton, J. R.; Preston, K. F. *Organometallics* **1985**, *4*, 1272.
(4) (a) Cooley, N. A.; Watson, K. A.; Fortier, S.; Baird, M. C. *Organometallics* **1986**, *5*, 2563. (b) Krusic, P. J.; McLain, S. J.; Morton, J. R.; Preston, K. F.; LePage, Y. *J. Magn. Reson.* **1987**, *74*, 72. (c) Morton, J. R.; Preston, K. F.; Cooley, N. A.; Baird, M. C.; Krusic, P. J.; McLain, S. J. *J. Chem. Soc., Faraday Trans. 1* **1987**, *83*, 3535. (d) Cooley, N. A.; Baird, M. C.; Morton, J. R.; Preston, K. F.; LePage, Y. *J. Magn. Reson.* **1988**, *76*, 325. (e) Fortier, S.; Baird, M. C.; Preston, K. F.; Morton, J. R.; Ziegler, T.; Jaeger, T.; Watkins, W. C.; MacNeil, J. H.; Watson, K. A.; Hensel, K.; LePage, Y.; Charland, J.-P.; Williams, A. J. *J. Am. Chem. Soc.* **1991**, *113*, 542.
(5) Hynes, R. C.; Preston, K. F.; Springs, J. J.; Williams, A. J. *Oranometallics* **1990**, *9*, 2298.
(6) (a) Kobayashi, T.; Yasufuku, K.; Iwai, J.; Noda, H.; Ohtani, H. *Coord. Chem. Rev.* **1985**, *64*, 1. (b) Church, S. P.; Hermann, H.; Grevels, F.-W.; Schaffner, K. *J. Chem. Soc., Chem. Commun.* **1984**, 785. (c) Church, S. P.; Poliakoff, M.; Timney, J. A.; Turner, J. J. *J. Am. Chem. Soc.* **1981**, *103*, 7515. (d) Howard, J. A.; Morton, J. R.; Preston, K. F. *Chem. Phys. Lett.* **1981**, *83*, 226. (e) Symons, M. C. R.; Sweaney, R. L. *Organometallics* **1982**, *1*, 834.
(7) (a) Meckstroth, W. K.; Walters, R. T.; Waltz, W. L.; Wojcicki, A.; Dorfman, L. M. *J. Am. Chem. Soc.* **1982**, *104*, 1842. (b) Yasufuku, K.; Noda, H.; Iwai, J.; Ohtani, H.; Hoshino, H.; Kobayashi, T. *Organometallics* **1985**, *4*, 2174. (c) Kobayashi, T.; Ohtani, H.; Noda, H.; Teratani, S.; Yamazaki, H.; Yasufuku, K. *Organometallics* **1985**, *5*, 110.

0002-7863/91/1513-9834$02.50/0

trigonal-bypyramidal (D_{3h}) structures, similar to the neutral 18-electron analogues $Fe(CO)_3L_2$.[12] Seemingly incongruent with this interpretation, however, is the observation of room temperature, liquid-phase EPR spectra, in which hyperfine coupling to two equivalent ^{31}P nuclei is readily resolved.[12] As pointed out previously,[2] if a species of the type $\{Fe(CO)_3L_2^+\}$ were to assume a structure of D_{3h} symmetry, the unpaired electron would occupy a degenerate e' level and a Jahn–Teller distortion would be anticipated. Unless the resultant splitting of the degenerate pair of levels were large, strong spin–orbital interaction between the erstwhile degenerate levels would result in very large g shifts and rapid relaxation of the electronic spin; the trigonal-bipyramidal variant would not be detectable by EPR spectroscopy except at very low temperatures in the frozen state.[13] Dynamic distortions or fluxionality at higher temperatures, which may result in an averaged D_{3h} structure, would render the EPR spectrum undetectably broad.

Thus the structural inferences from EPR and IR spectroscopy for species of the type $\{Fe(CO)_3L_2^+\}$ are in conflict. In an attempt to resolve this anomaly, we have grown crystals of the complex $[Fe(CO)_3(PPh_3)_2][PF_6]\cdot{}^1/_2CH_2Cl$ and have determined the X-ray crystal structure. In order to examine the EPR spectrum, we have also doped the cation $\{Fe(CO)_3(PPh_3)_2^+\}$ to the extent of $\approx 1\%$ into crystals of the known[14] $[Co(CO)_3(PPh_3)_2][PF_6]\cdot CH_2Cl_2$, the crystal structure of which was also determined. Finally, for purposes of comparison, we have carried out density functional calculations on the species $\{M(CO)_3L_2\}$ (M = Mn, Fe^+; L = CO, PH_3).

Experimental Section

Syntheses and X-ray Crystal Structure Determinations. All operations were carried out under an inert nitrogen atmosphere using standard Schlenk techniques or a Vacuum Atmospheres glovebox. Dichloromethane was refluxed under nitrogen with CaH_2 for at least 48 h prior to use while hexanes were distilled from sodium and a benzophenone indicator. All solvents were further N_2 saturated by steady bubbling for at least 20 min immediately before use. The complexes $[Co(CO)_3(PPh_3)_2]PF_6\cdot CH_2Cl_2$[14] and $[Fe(CO)_3(PPh_3)_2]PF_6\cdot{}^1/_2CH_2Cl_2$[12a] were prepared by published methods.

Yellow crystals of $[Co(CO)_3(PPh_3)_2]PF_6\cdot CH_2Cl_2$ were obtained through layered diffusion of hexane into a dichloromethane solution at ambient temperature. A suitable crystal was mounted with epoxy on a glass fiber. The initial space-group determination was done using a Buerger Precession Camera, while subsequent diffraction work was performed on an Enraf-Nonius CAD-4 diffractometer using Mo Kα graphite-monochromated X-ray radiation. A $\omega/2\theta$ data collection was carried out at room temperature, with intensity and orientation standards showing no significant variation over the length of the data aquisition period. The data were corrected for Lorentz and polarization effects; absorption corrections were not considered necessary. The structure was solved through direct methods using the XTAL 3.0 program package[15] on a Sun SPARCStation 1. Difference Fourier maps revealed the location of 26 of the hydrogen atoms. The positions of the remaining four hydrogens were calculated and inserted into the solution. Each hydrogen was assigned the isotropic temperature factor of its parent atom. Full-matrix least-squares refinement[16] of positional and thermal parameters for all heavy atoms included all reflections having $I > 3\sigma(I)$. In the final cycles of refinement, anisotropic temperature factors were employed; 496 variable parameters converted to give agreement factors $R = 5.0\%$ and $R_w = 5.2\%$. Further crystallographic details are listed in Table I, and pertinent bond lengths and angles are compiled in Table II. Complete listings of positional parameters and equivalent thermal parameters are deposited as Supplementary Material.

Deep green crystals of $[Fe(CO)_3(PPh_3)_2]PF_6\cdot{}^1/_2CH_2Cl_2$ were grown through layered diffusion of hexane into a dichloromethane solution at −35 °C in the glovebox. Although very unstable in solution at room temperature, the compound is stable for days both in solution at −35 °C and in the solid state at room temperature in the dark. A suitable crystal was mounted with epoxy on a glass fiber and sealed in a glass capillary under an inert nitrogen atmosphere. X-ray data were collected on an Enraf-Nonius CAD-4 diffractometer using Mo Kα graphite monochromated X-ray radiation. The unit cell was determined from 25 well-centered reflections. A $\omega/2\theta$ data collection was carried out at room temperature, with intensity and orientation standards showing no significant variation. The data were collected in two shells, the first with

Table I. Crystallographic Data for $[Co(CO)_3(PPh_3)_2]PF_6\cdot CH_2Cl_2$ and $[Fe(CO)_3(PPh_3)_2]PF_6\cdot{}^1/_2CH_2Cl_2$

molecular formula	$C_{40}H_{32}Cl_2CoF_6O_3P_3$	$C_{39}H_{30}F_6FeO_3P_3\cdot{}^1/_2CH_2Cl_2$
molecular weight	897.44	851.64
space group	$P2_1/n$ (no. 14)	$P\bar{1}$ (no. 2)
a, Å	17.155 (9)	18.694 (9)
b, Å	13.753 (4)	11.434 (5)
c, Å	17.457 (10)	10.915 (2)
α, deg		63.40 (3)
β, deg	104.01 (4)	104.71 (3)
γ, deg		109.49 (4)
vol, Å^3	3996.2	1939.99
Z	4	2
μ, cm^{-1}	0.769	0.662
density, g cm^{-3}	1.492	1.457
T, K	292	292
crystal dimens, mm	0.50 × 0.40 × 0.15	0.40 × 0.35 × 0.20
$F(000)$	1824	868
λ(Mo Kα)	0.710732	0.710732
2θ range scanned (deg)	1.0, 40.0	1.0, 50.0
sin θ/λ max	0.4821	0.624
h, k, l range obsd	−16 → 16, 0 → 13, 0 → 16	0 → 23, −13 → 12, −12 → 12
no. of unique reflcns	3741	6091
no. of obsd reflcns	2580	2290
final R, R_w	0.050, 0.052	0.053, 0.058
largest shift/error in final least-squares cycle, δ/σ	0.003	0.04
max and min residual electron density in final Fourier map, e/Å^3	1.14, −0.70	3.62, −2.05

Table II. Selected Bond Distances (Å) and Angles (deg) for $[Co(CO)_3(PPh_3)_2]PF_6\cdot CH_2Cl_2$

Distances

Co–P(1)	2.239 (5)	P(1)–C(1A)	1.804 (8)	C(1)–O(1)	1.13 (1)
Co–P(2)	2.240 (5)	P(1)–C(7A)	1.811 (9)	C(2)–O(2)	1.16 (1)
Co–C(1)	1.81 (1)	P(1)–C(13A)	1.806 (9)	C(3)–O(3)	1.15 (1)
Co–C(2)	1.75 (1)	P(2)–C(1B)	1.794 (8)		
Co–C(3)	1.775 (9)	P(2)–C(7B)	1.822 (9)		
		P(2)–C(13B)	1.807 (9)		

Angles

P(1)–Co–P(2)	176.5 (1)	C(1)–Co–C(3)	119.5 (4)
P(1)–Co–C(1)	92.0 (3)	C(2)–Co–C(3)	122.7 (5)
P(1)–Co–C(2)	90.0 (4)	Co–P(1)–C(1A)	114.4 (3)
P(1)–Co–C(3)	87.9 (3)	Co–P(2)–C(1B)	115.3 (3)
P(2)–Co–C(1)	91.1 (3)	Co–C(1)–O(1)	178.6 (7)
P(2)–Co–C(2)	90.2 (4)	Co–C(2)–O(2)	179.7 (9)
P(2)–Co–C(3)	89.1 (3)	Co–C(3)–O(3)	177.3 (9)
C(1)–Co–C(2)	117.8 (4)		

(8) (a) Lionel, T.; Morton, J. R.; Preston, K. F. *J. Chem. Phys.* **1982**, *76*, 234. (b) Peake, B. M.; Symons, M. C. R.; Wyatt, J. L. *J. Chem. Soc., Dalton Trans.* **1983**, 1171. (c) Lionel, T.; Morton, J. R.; Preston, K. F. *J. Magn. Reson.* **1982**, *49*, 225.

(9) (a) Elian, M.; Hoffmann, R. *Inorg. Chem.* **1975**, *14*, 1058. (b) Rossi, A. R.; Hoffmann, R. *Inorg. Chem.* **1975**, *14*, 365.

(10) (a) Kidd, D. R.; Cheng, C. P.; Brown, T. L. *J. Am. Chem. Soc.* **1978**, *100*, 4103. (b) McCullen, S. B.; Brown, T. J. *J. Am. Chem. Soc.* **1982**, *104*, 7496. (c) Walker, H. W.; Rattinger, G. B.; Belford, R. L.; Brown, T. L. *Organometallics* **1983**, *2*, 775. (d) Walker, H. W.; Herrick, R. S.; Olsen, R. J.; Brown, T. L. *Inorg. Chem.* **1984**, *23*, 3748.

(11) Crocker, L. S.; Heinekey, D. M.; Schulte, G. K. *J. Am. Chem. Soc.* **1989**, *111*, 405.

(12) (a) Baker, P. K.; Connolly, N. G.; Jones, B. M. R.; Maher, J. P.; Somers, K. R. *J. Chem. Soc., Dalton Trans.* **1980**, 579. (b) Blanch, S. W.; Bond, A. M.; Colton, R. *Inorg. Chem.* **1981**, *20*, 755. (c) Bagchi, R. N.; Bond, A. M.; Heggie, C. L.; Henderson, T. L.; Mocellin, E.; Seikel, R. A. *Inorg. Chem.* **1983**, *22*, 3007. (d) Therien, M. J.; Ni, C.-L.; Anson, F. C.; Osteryoung, J. G.; Trogler, W. C. *J. Am. Chem. Soc.* **1986**, *108*, 4037. (e) Therien, M. J.; Trogler, W. C. *J. Am. Chem. Soc.* **1986**, *108*, 3697.

(13) McGarvey, B. R. *Transition Met. Chem.* **1966**, *3*, 89.

(14) Lee, K. Y.; Kochi, J. K. *Inorg. Chem.* **1989**, *28*, 567.

(15) Hall, S. R., Stewart, J. M., Eds. *Xtal User'ss Reference Manual-Version 3.0*; Universities of Western Australia and Maryland, 1990.

(16) The function being minimized was $\sum_h w(|F_o| - |F_c|)^2$, where $w^{-1} = \sigma F_o$.

Table III. Selected Bond Distances (Å) and Angles (deg) for $[Fe(CO)_3(PPh_3)_2]PF_6 \cdot {}^1/_2CH_2Cl_2$

Distances					
Fe–P(1)	2.282 (4)	P(1)–C(1A)	1.79 (1)	C(1)–O(1)	1.14 (2)
Fe–P(2)	2.283 (3)	P(1)–C(7A)	1.81 (1)	C(2)–O(2)	1.13 (1)
Fe–C(1)	1.80 (1)	P(1)–C(13A)	1.82 (1)	C(3)–O(3)	1.13 (1)
Fe–C(2)	1.80 (1)	P(2)–C(1B)	1.804 (9)		
Fe–C(3)	1.81 (1)	P(2)–C(7B)	1.83 (1)		
		P(2)–C(13B)	1.82 (1)		

Angles			
P(1)–Fe–P(2)	163.4 (1)	C(1)–Fe–C(3)	101.4 (6)
P(1)–Fe–C(1)	99.2 (4)	C(2)–Fe–C(3)	162.0 (6)
P(1)–Fe–C(2)	88.4 (4)	Fe–P(1)–C(1A)	114.5 (3)
P(1)–Fe–C(3)	87.4 (4)	Fe–P(2)–C(1B)	111.9 (4)
P(2)–Fe–C(1)	97.4 (4)	Fe–C(1)–O(1)	179 (1)
P(2)–Fe–C(2)	89.1 (4)	Fe–C(2)–O(2)	177 (1)
P(2)–Fe–C(3)	89.9 (4)	Fe–C(3)–O(3)	179 (1)
C(1)–Fe–C(2)	96.6 (5)		

$\theta \leq 40°$ and the second with $40° < \theta \leq 50°$. The two data sets were combined prior to structure solution.

The data were corrected for Lorentz and polarization effects, and the structure was solved with direct methods in the XTAL 3.0 program package[15] on a Sun SPARCStation 1 to reveal all non-hydrogen atoms in the $Fe(CO)_3(PPh_3)_2^+$ and PF_6^- structures, as well as the two chlorine atoms of the dichloromethane hemi-solvate. A disorder problem prohibited location of the methylene carbon atom. The solution was refined isotropically following which the positions of the hydrogens were calculated and inserted with the isotropic displacement parameter of their parent atoms. Full-matrix least-squares refinement of positional and anisotropic thermal parameters was carried out for all heavy atoms. This refinement employed 478 variables and included 2290 reflections with $I > 3\sigma(I)$; it converged to yield agreement factors of $R = 5.3\%$ and $R_w = 5.8\%$. Further crystallographic datails are presented in Table I, and pertinent bond lengths and angles are compiled in Table III. Complete listings of positional parameters and equivalent thermal parameters are deposited as Supplementary Material.

Single-Crystal EPR. Single crystals of the diamagnetic cobalt compound doped with ≈1% of the iron radical cation were grown with the hexane/dichloromethane diffusion method at −35 °C in the dark. Single crystals of suitable size for EPR spectroscopy were selected with the aid of a polarizing microscope and orientated on a Picker diffractometer according to the structural parameters of the pure cobalt host (Table I). Once in the desired orientation, these crystals were glued with epoxy cement into the ends of 4 mm o.d. quartz tubes such that one of the orthogonal axes a^*bc[17] of the $P2_1/n$ monoclinic crystal lay parallel to the tube axis. A pointer glued at right angles to the tube axis was used to indicate the direction of a second crystal axis. The tube and affixed crystal were held in a Dewar of liquid nitrogen with the crystal positioned at the center of the resonant rectangular microwave cavity of a Varian E12 spectrometer and the pointer placed immediately above a horizontal brass protractor. EPR spectra were recorded and measured as a function of angle throughout three orthogonal crystal planes and for the skew direction $(1/\sqrt{3}, 1/\sqrt{3}, 1/\sqrt{3})$ in order to characterize the monoclinic unit cell.[18] The same resonant cavity could also be equipped with special Dewar inserts for the measurement of powder and solution spectra at temperatures between 4 and 400 K. Magnetic field measurements were made with a Bruker ER035M gaussmeter, and microwave frequencies were determined with a Systron-Donner counter.

Computational Details. The calculations were all based on the Hartree-Fock-Slater (HFS) model as implemented by Baerends[19] et al., and utilized the latest version of the fully vectorized HFS-LCAO-STO program of Ravenek.[20] Energy differences were calculated by the generalized transition-state method[21] in conjunction with Becke's[22a] non-local exchange corrections as well as corrections to allow for correlations between electrons of different spins.[23] The numerical integration scheme employed in this work was formulated by Becke.[22b]

An uncontracted triple-ζ STO basis set[24] was used for iron and manganese. The ligand atoms were described by a double-ζ STO basis[24] set which was extended with one polarization function (2p on H and 3d on C, O and P). The electrons in the shells of lower energy on metal, C, and O atoms were considered as core electrons and treated by the frozen-core approximation according to Baerends et al.[19,24] The geometry optimizations were carried out at the HFS level of theory according to the algorithm developed by Versluis and Ziegler.[25]

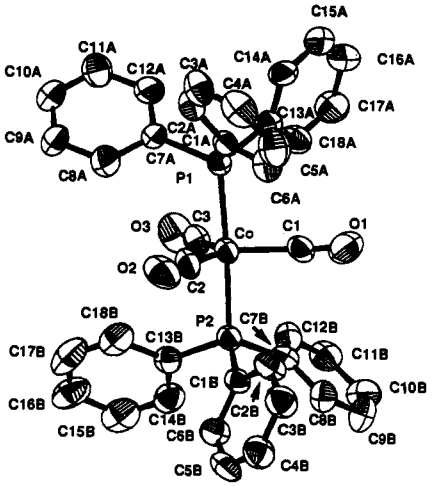

Figure 1. ORTEP drawing of $[Co(CO)_3(PPh_3)_2][PF_6] \cdot CH_2Cl_2$.

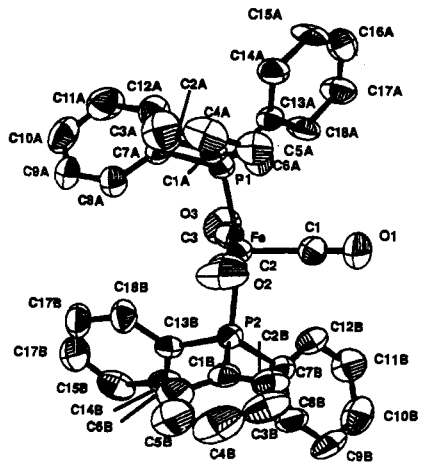

Figure 2. ORTEP drawing of $[Fe(CO)_3(PPh_3)_2][PF_6] \cdot {}^1/_2CH_2Cl_2$.

Results and Discussion

Description of the Crystal Structures. Figure 1 shows an ORTEP of the complex cation of the cobalt compound $[Co(CO)_3(PPh_3)_2]PF_6 \cdot CH_2Cl_2$; the important bond lengths and angles are listed in Table II. The compound consists of discrete cations and anions, with the former assuming an essentially trigonal-bipyramidal structure with axial phosphines (P–Co–P bond angle 176.5 (1)°) and equatorial carbonyl groups (OC–Co–CO bond angles 117.8 (4)°, 119.5 (4)°, and 122.7 (5)°). Although no crystal structures of complexes of the type $[Co(CO)_3L_2^+]$ appear to have been previously reported, we note that the Co–CO and C–O bond lengths of $[Co(CO)_3(PPh_3)_2]PF_6 \cdot CH_2Cl_2$ are comparable with those of the cationic complex $[Co(CO)_2(PMe_3)_3]BPh_4$[26a] but

(17) Rollett, J. S. *Computing Methods in Crystallography*; Pergamon: London, 1965; Chapter 3.
(18) Morton, J. R.; Preston, K. F. *J. Magn. Reson.* **1983**, *52*, 457.
(19) (a) Baerends, E. J.; Ellis, D. E.; Ros, P. *Chem. Phys.* **1973**, *2*, 41. (b) Baerends, E. J., Ph.D. Thesis, 1975, Vrije Universiteit, Amsterdam.
(20) Ravenek, W. In *Algorithms and Applications on Vector and Parallel Computers*; Riele, H. J. J., Dekker, Th. J., van der Vorst, H. A., Eds.; Elsevier: Amsterdam, 1987.
(21) (a) Ziegler, T.; Rauk, A. *Theor. Chim. Acta* **1977**, *46*, 1. (b) Ziegler, T. Ph.D. Thesis, 1978, University of Calgary, Calgary, Canada.
(22) (a) Becke, A. D. *J. Chem. Phys.* **1986**, *84*, 4524. (b) Becke, A. D. *J. Chem. Phys.* **1988**, *88*, 2547.
(23) (a) Stoll, H.; Pavlidou, C. M. E.; Preuss, H. *Theor. Chim. Acta* **1978**, *49*, 143. (b) Stoll, H.; Golka, E.; Preuss, H. *Theor. Chim. Acta* **1980**, *55*, 29.
(24) (a) Snijders, G. J.; Baerends, E. J.; Vernooijs, P. *At. Nucl. Data Tables* **1982**, *26*, 483. (b) Vernooijs, P.; Snijders, G. J.; Baerends, E. J. *Slater Type Basis Functions for the whole Periodic System*; Internal report, Free University of Amsterdam, The Netherlands, 1981.
(25) Versluis, L.; Ziegler, T. *J. Chem. Phys.* **1988**, *88*, 322.

Table IV. The $\mathbf{g}^2$ and $\mathbf{g}\cdot\mathbf{a}^2\cdot\mathbf{g}$ (MHz^2) Matrices for $\{Fe(CO)_3(PPh_3)_2^+\}$ in a Crystal of $[Co(CO)_3(PPh_3)_2][PF_6]\cdot CH_2Cl_2$ and Principal Values of **g** and Hyperfine Interaction[a] (MHz) and Their Direction Cosines in the a^*bc Axis System

				principal values and direction cosines of **g** and **a**		
	a^*	b	c	x	y	z
				2.0795	2.0898	2.0091
$\mathbf{g}^2$	4.3356	±0.0142	0.0749	0.5408	0.8064	−0.2394
	±0.0142	4.2818	∓0.1126	±0.8074	∓0.4179	±0.4164
	0.0749	∓0.1126	4.1103	−0.2358	0.4185	0.8771
				61.2	49.9	50.7
$\mathbf{g}\cdot\mathbf{a}^2\cdot\mathbf{g}$[a]	12003	±2141	−551	0.4655	0.8260	−0.3179
	±2141	14631	∓1346	±0.8474	∓0.3124	±0.4293
	−551	∓1346	10816	−0.2553	0.4692	0.8454

[a] Hyperfine interactions (MHz) and matrix components (MHz^2) for two equivalent ^{31}P nuclei.

longer and shorter, respectively, than those of the neutral $HCo(CO)(PPh_3)_3$.[26b] The Co–P bond lengths of $[Co(CO)_3(PPh_3)_2]PF_6\cdot CH_2Cl_2$ are also longer than those of $HCo(CO)(PPh_3)_3$.[26b]

Figure 2 shows an ORTEP of $[Fe(CO)_3(PPh_3)_2]PF_6\cdot{}^1/_2CH_2Cl_2$; the important bond lengths and angles are listed in Table III. The unit cell contains two cations, two anions, and one molecule of the solvent, thus accounting for the original finding that this complex is a hemi-solvate.[12a] Although disorder in the site occupations of the dichloromethane molecules resulted in uncertainty concerning the exact positions of the solvent molecule atoms, the positions of all non-hydrogen atoms of the cation and anion were determined completely satisfactorily. The crystals were not, in fact, of high quality, a fact evident from the large number of unobserved reflections, especially in the $40° \le 2\theta \le 50°$ range (Table I). Data refinement excluding these later reflections generated essentially the same solution, however with no significant improvement in the R value or standard deviations. Large electron density residuals also remain associated with the heavy atom center, but despite these problems, the positions of all other non-hydrogen atoms of the cation and the anion were determined completely satisfactorily.

The octahedral PF_6^- counterion is positioned well off the pseudo-4-fold axis of the cation, such that the shortest Fe–F distance is 4.331 Å; thus the anion is sited well beyond the inner coordination sphere of the iron. The cation may be best considered a distorted square pyramid with trans, basal triphenylphosphines (P–Fe–P bond angle 163.4 (1)°) and a meridional arrangement of carbonyl groups ((basal CO)–Fe–(basal CO) bond angle 162.0 (6)°; (axial CO)–Fe–(basal CO) bond angles 101.4 (6)° and 96.6 (5)°). The bond angles are thus all very different from those of the essentially trigonal-bipyramidal $[Co(CO)_3(PPh_3)_2^+]$ and are, in fact, very similar to those reported for the distorted square-pyramidal $\{Re(CO)_3(PCy_3)_2\}$.[11]

The Fe–CO and Fe–P bond lengths are slightly larger than are the corresponding metal–ligand bond lengths of the cobalt cation, $[Co(CO)_3(PPh_3)_2^+]$. The Fe–CO bond lengths are marginally longer than the axial and equatorial Fe–C bond lengths of $Fe(CO)_4PPh_3$[27a] and are comparable with the axial Fe–C bond lengths of $Fe(CO)_5$,[27b] but are significantly shorter than the equatorial Fe–C bond lengths of the latter compound.[27b] The Fe–P bond lengths of $[Fe(CO)_3(PPh_3)_2^+]$ are slightly longer than that of $Fe(CO)_4PPh_3$.[27a]

EPR Spectroscopic Study. For a random orientation of the dc magnetic field of the spectrometer with respect to a single crystal of $[Co(CO)_3(PPh_3)_2][PF_6]\cdot CH_2Cl_2$ doped with $[Fe(CO)_3(PPh_3)_2][PF_6]$, the EPR spectrum at 77 K consisted of two sets of equally intense 1:2:1 triplets (Figure 3). Coalescences to a single 1:2:1 triplet occurred along the crystal axes and throughout the a^*c plane, showing that the doublet splitting was due to two

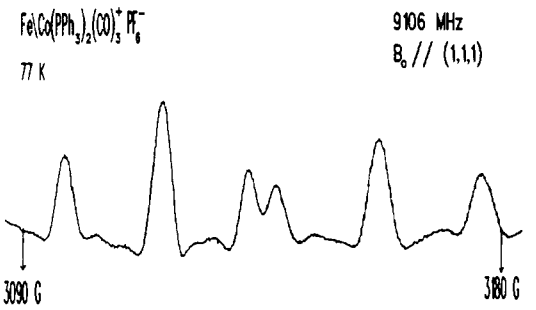

Figure 3. Second-derivative EPR spectrum at 77 K of $[Fe(CO)_3(PPh_3)_2^+]$ in a $[Co(CO)_3(PPh_3)_2][PF_6]$ crystal for the skew $(1/\sqrt{3}, 1/\sqrt{3}, 1/\sqrt{3})$ direction of the magnetic field.

magnetically inequivalent sites related by the symmetry operations of the monoclinic crystal.[18] The 1:2:1 pattern associated with each site was preserved for all orientations, with no indication of splitting of the central feature to give a 1:1:1:1 intensity pattern. Accordingly, this manifold was attributed to hyperfine interactions with two equivalent ^{31}P ($I = {}^1/_2$) nuclei. Anisotropies in the electronic Zeeman interaction, **g**, and in the equal hyperfine interactions, $\mathbf{a}(^{31}P)$, were quantified in the established manner[18] via assembly of the $\mathbf{g}\cdot\mathbf{g}$ and $\mathbf{g}\cdot\mathbf{a}\cdot\mathbf{a}\cdot\mathbf{g}$ matrices (Table IV). Best estimates of the elements of these matrices were obtained[18] from least-squares fits of sine curves to the measures of g^2 and g^2a^2 made at regular intervals throughout the a^*b, a^*c, and bc crystal planes (Supplementary Material), and along the skew $(1/\sqrt{3}, 1/\sqrt{3}, 1/\sqrt{3})$ direction. Standard algebraic procedures[16] were used to obtain the principal values and directions for **g** and $\mathbf{a}(^{31}P)$ given in Table IV.

The spectrum of a finely powdered sample of iron-doped crystals was recorded at temperatures from 4 K up to ambient. At temperatures up to that of liquid nitrogen, the spectrum showed little change in appearance; it was (Supplementary Material) the polycrystalline spectrum anticipated for the **g** and $\mathbf{a}(^{31}P)$ matrices derived from the single-crystal measurements (Table IV). Simulation[28] using the principal values of **g** and **a** derived from the single-crystal study (Table IV) reproduced the observed spectrum well, with the exception of a few weak features; the latter were all orientation dependent, and were therefore attributed to small crystals remaining in the powdered sample. At temperatures above ≈80 K, the polycrystalline spectrum narrowed with increase of temperature (Supplementary Material); the hyperfine manifolds associated with the smallest and largest g components broadened and moved toward each other, while the g_{inl} manifold initially remained sharp, but also broadened at temperatures approaching ambient. At room temperature, the spectrum consisted of a single featureless line with a p–p width of ≈80 G and $g = 2.055$.

For purposes of comparison with earlier work,[12a,c,e] we examined both liquid and frozen solutions (Supplementary Material) of

(26) (a) Pēr̄ès, Y.; Kerkeni, A.; Dartiguenave, M.; Dartiguenave, Y.; Bēlanger-Gariēpy, F.; Beauchamp, A. L. *J. Organomet. Chem.* **1987**, *323*, 397. (b) Whitfield, J. M.; Watkins, S. F.; Tupper, G. B. *J. Chem. Soc., Dalton Trans.* **1977**, 407.

(27) (a) Riley, P. E.; Davis, R. E. *Inorg. Chem.* **1980**, *19*, 159. (b) Beagley, B.; Schmidling, D. G. *J. Mol. Struct.* **1974**, *22*, 466.

(28) Belford, R. L.; Nilges, M. J. *Computer Simulation of Powder Spectra*; EPR Symposium, 21st Rocky Mountain Conference, Denver, CO, 1979.

Table V. Spectral Parameters of $\{Fe(CO)_3(PPh_3)_2^+\}$ Estimated from Liquid and Solid Polycrystalline Samples

matrix	T (K)	g_{xx} a_{xx}[b]	g_{yy} a_{yy}	g_{zz} a_{zz}	g_{av}[a] a_{av}[a]	ref
Co crystal	77	2.0795	2.0898	2.0091	2.0595	this work
		61.2	49.9	50.7	53.9	
Co powder	77	2.0791	2.0888	2.0085	2.0588	this work
		58.2	50.6	48.8	52.6	
	297				2.0554	this work
CH_2Cl_2	77	2.0530	2.0891	2.0013	2.0478	this work
		60.3	45.7	57.7	54.6	
	?[c]	2.055	2.089	2.004	2.049	12a
		d	*d*	*d*		
	298				2.050	12a
					53.1	
	300				2.053	12e
					54.0	
	293				2.052	12c
					56.0	

[a] Average of the three tensor components, or the isotropic value for liquids. [b] Hyperfine interaction (MHz) for two equivalent ^{31}P nuclei. [c] Temperature not given. [d] Hyperfine structure not resolved at Q-band frequency.

Table VI. Correlation between Tensor Principal Directions and Certain Bond Directions within the Host Cation

	angle (deg) to		
principal value	Co–C(1)	P(1)–P(2)	⊥r C(1)CoP(1)P(2)
g_{min} = 2.0091	1.3	89.6	88.6
g_{int} = 2.0795	89.7	7.0	97.0
g_{max} = 2.0898	91.4	83.0	7.0
a_{min} = 49.9 MHz	86.6	87.8	4.0
a_{int} = 50.7 MHz	3.4	91.1	86.6
a_{max} = 61.2 MHz	89.2	2.5	87.9

$[Fe(CO)_3(PPh_3)_2][PF_6]$ in pure, dry dichloromethane. A summary of spectral parameters for $\{Fe(CO)_3(PPh_3)_2^+\}$ is given in Table V. Our estimates of the principal values of **g** and **a**(^{31}P) derived from polycrystalline or glassy samples were obtained from turning points[29] in the first-derivative spectra.

The observation of spectra from two magnetically inequivalent sites which coalesced when B_0 lay along *b* or in *ac* showed that the impurity paramagnet in $[Co(CO)_3(PPh_3)_2][PF_6]\cdot CH_2Cl_2$ obeyed the host crystal symmetry. It therefore seemed very likely that the dopant $\{Fe(CO)_3(PPh_3)_2^+\}$ was a substitutional impurity with the diamagnetic host. Analysis based on this assumption led to principal directions of **g** and **a**(^{31}P) for the two equivalent ^{31}P nuclei (Table IV) which correlated very well with certain bond directions (Table VI) within the host cation. Furthermore, one-third of the traces of the **g** and **a**(^{31}P) matrices agreed very well with previous (Table V) isotropic parameters attributed to $\{Fe(CO)_3(PPh_3)_2^+\}$ and so left little doubt about the identity of the signal carrier in the single crystals. There was a significant difference between the intermediate principal value of **g** determined for the crystal of $[Co(CO)_3(PPh_3)_2][PF_6]\cdot CH_2Cl_2$ and the value estimated[12a] from analysis of a Q-band powder spectrum in frozen dichloromethane. Our own analyses (Table V) of powder spectra in both matrices supported the determinations of g_{int} and confirmed the existence of a substantial matrix dependence of that principal value.

Considering first the **g** matrix, we note that it is nearly uniaxial, with both a unique principal value not too far removed from the free-spin *g* factor (2.0023) and other components considerably in excess of that value. The principal values are very reminiscent of those established for the iron pentacarbonyl radical cation and related species.[6d,e,8a,30a–d] It is now established beyond all reasonable doubt[5–11,30] that such species have a *square-pyramidal* geometry; they are low-spin d^7 species in which the unpaired electron resides principally in a metal valence $sp_zd_{z^2}$ hybrid orbital.[9a] Spin–orbit interactions between the a_1 (in C_{4v}) semioccupied orbital (SOMO) and a nearby filled degenerate pair (*xz*, *yz*) results in substantial positive deparatures of g_{xx} and g_{yy} from the free-spin value. However, the absence of metal orbitals of appropriate symmetry (A_2 in C_{4v}) precludes spin–orbit interaction with the SOMO when $B_0 \| z$, and limits the principal *g* value along the symmetry axis (g_{zz}) to values close to 2.0023. In C_{2v} symmetry (Figure 4), this restriction is relaxed and small positive shifts in

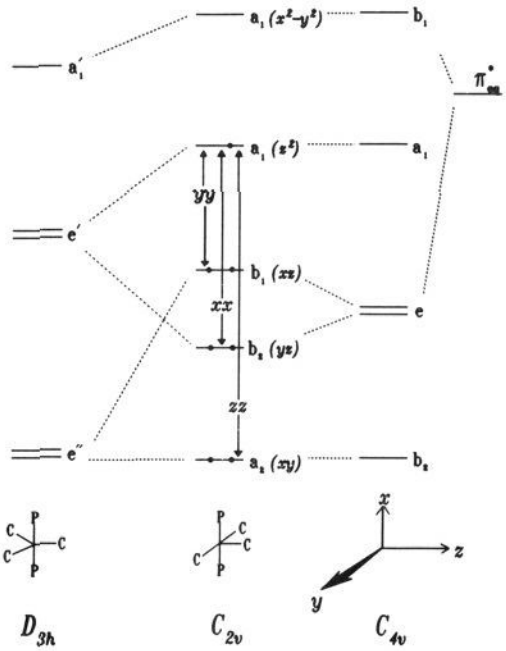

Figure 4. d-orbital energy-level scheme for $\{Fe(CO)_3(PPh_3)_2^+\}$, showing the effects of basal-CO π^* orbitals.

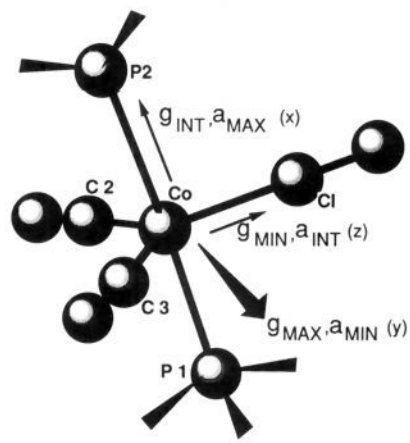

Figure 5. Location of the principal values of **g** and **a**(^{31}P) within the structure of the host cation.

(29) Atkins, P. W.; Symons, M. C. R. *The Structure of Inorganic Radicals*; Elsevier: Amsterdam, 1967; p 269.

(30) (a) Symons, M. C. R.; Morton, J. R.; Preston, K. F. In *High Energy Processes in Organometallic Chemistry*; Suslick, K. S., Ed.; American Chemical Society: Washington, DC, 1987; ACS Symp. Ser. No. 333, p 169. (b) Fairhurst, S. A.; Morton, J. R.; Perutz, R. N.; Preston, K. F. *Organometallics* **1984**, *3*, 1389. (c) Rattinger, G. B.; Belford, R. L.; Walker, H.; Brown, T. L. *Inorg. Chem.* **1989**, *28*, 1059. (d) Morton, J. R.; Preston, K. F.; Darensbourg, M. Y. *Magn. Res. Chem.* **1988**, *26*, 787. (e) Krusic, P. J.; Cote, W. J.; Grand, A. *J. Am. Chem. Soc.* **1984**, *106*, 4642. (f) Morton, J. R.; Preston, K. F.; Le Page, Y.; Krusic, P. J. *J. Chem. Soc., Faraday Trans. 1* **1989**, *85*, 4019. (g) Krusic, P. J.; Baker, R. T.; Calabrese, J. C.; Morton, J. R.; Preston, K. F.; Le Page, Y. *J. Am. Chem. Soc.* **1989**, *111*, 1262. (h) Horrocks, W. D.; van Hecke, G. R.; Hall, D. D. *Inorg. Chem.* **1967**, *6*, 694. (i) Stalick, J. K.; Corfield, P. W. R.; Meek, D. W. *Inorg. Chem.* **1973**, *12*, 1668. (j) Fairhurst, S. A.; Morton, J. R.; Preston, K. F. *J. Magn. Reson.* **1983**, *55*, 453.

g_{zz} may arise, providing the $a_1(z^2)$ orbital acquires some $d_{x^2-y^2}$ character. In the case of $\{Fe(CO)_3(PPh_3)_2^+\}$ trapped in $[Co(CO)_3(PPh_3)_2][PF_6]\cdot CH_2Cl_2$ crystals, the principal value which we have labeled g_{zz} is close to the free-spin value and lies parallel, within experimental error, to the host cation Co–C(1) bond (Table VI, Figure 5). We reach the inescapable conclusion that this radical has the same basic structure as the parent iron pentacarbonyl cation radical, i.e. square pyramidal with the unique axis directed along one of the equatorial bonds of the host cation. Widening of C(2)–M–C(3) has presumably taken place on substitution of Fe for Co, resulting in a lowering of symmetry from D_{3h} in the host cation to C_{2v} in the radical. In C_{2v} symmetry, the principal directions of **g** are dictated by the symmetry elements: two mirror planes and a 2-fold axis. It is with some satisfaction therefore that we note the close correlation of the principal directions of the remaining g values, g_{xx} and g_{yy}, with P(1)–P(2) and with the perpendicular to the C(1)CoP(1)P(2) plane, respectively (Table VI, Figure 5).

In a low-spin d^7 trigonal-bipyramidal species, the unpaired electron would occupy the degenerate (d_{xy}, $d_{x^2-y^2}$) levels, and the ground-state electronic configuration would be $(e'')^4(e')^3$.[9] Such a molecule is subject to a Jahn–Teller distortion which lifts the degeneracy of the ground state. Unless this distortion is exceptionally large, the erstwhile degenerate levels will not differ greatly in energy and will interact strongly in the presence of the dc magnetic field via spin–orbit coupling. Strong spin–orbit interaction has two practical consequences for EPR spectroscopy: short spin–lattice relaxation times and large g shifts. The former consequence translates into undetectably broad spectra at elevated temperatures, and in the liquid state in particular. Such is certainly not the case for the radical under study here.[12a,c,e] The second consequence of strong spin–orbit coupling provides much more compelling evidence against a trigonal-bipyramidal structure for $\{Fe(CO)_3(PPh_3)_2^+\}$. In geometries approaching D_{3h}, a large positive g shift is anticipated along the 3-fold axis of the undistorted structure, and much smaller shifts when B_0 lies in the equatorial plane. Such a disposition of principal g values has indeed been observed for trigonal-bipyramidal geometries[30e-j] but does *not* fit the present experimental observations.

The near equality of the in-plane g values, g_{xx} and g_{yy}, for $\{Fe(CO)_3(PPh_3)_2^+\}$ is surprising at first sight, but is in line with observations for other metal carbonyl phosphine radicals[5,30] and has been rationalized elsewhere.[5] The shifts in g (Figure 4) from the free-spin value are given approximately by

$$\Delta g = 6\lambda\rho_1\rho_2/\Delta E \qquad (1)$$

where λ is the spin–orbit coupling constant for the metal nucleus, ΔE is the energy difference between the d_{z^2} and the appropriate, filled (d_{xz}, d_{yz}) level, and ρ_1 and ρ_2 are the unpaired spin densities in the ground and excited states. A rough estimate of ΔE from the λ value[31] for Fe^+ and the assumption of unit spin density at the metal nucleus in the two interacting orbitals shows that it is a large term, $\cong 26\,000$ cm^{-1}. This is not surprising since the interacting orbitals have distinct origins in the widely separated e_g and t_{2g} levels of O_h symmetry.[32] The separation of a_1 from the b_1, b_2 pair is determined to first order by σ-bonding: CO and phosphines are almost equally strong σ-donors, so that b_1 and b_2 are strongly stabilized with respect to a_1, but remain proximate. Their separation and the ordering of the g_{xx} and g_{yy} values is readily rationalized in terms of π-bonding differences in the equatorial plane of the proposed $^2A_1$ (in C_{2v}) structure; phosphines are poor π-acceptors compared to carbon monoxide.[33] Interaction of the π^* orbitals of equatorial CO ligands (Figure 4) stabilizes the filled d_{xz} and d_{yz} orbitals; the absence of such stabilization from P $3p_z$ in $\{Fe(CO)_3(PPh_3)_2^+\}$ (Fe–P along x) leaves the d_{xz} level above d_{yz}. Since the g shift along x is generated by spin–orbit interaction between d_{z^2} and d_{yz}, it will therefore be a smaller departure from the free-spin value than Δg_{yy}, as observed (Figure 4).

The pronounced matrix dependence of the intermediate g value, g_{xx}, is readily accounted for in terms of this model. In the $[Co(CO)_3(PPh_3)_2][PF_6]\cdot CH_2Cl_2$ crystal, we can safely assume that the C(2)–Fe–C(3) angle will be substantially less than 180°. The X-ray crystal structure determination of $[Fe(CO)_3(PPh_3)_2][PF_6]\cdot{}^1/_2CH_2Cl_2$ reported here certainly supports such an assumption. Thus overlap of the C(2) and C(3) p_z orbitals with Fe $3d_{yz}$ will be less efficient than for a linear arrangement of C(2)–Fe–C(3). Solvents may tend to associate with the radical by occupying the empty octahedral site; it has been argued that such an interaction of the radical SOMO with a ligand lone pair would be partially stabilizing.[1b] Enlargement of the C(2)–Fe–C(3) angle, which would undoubtedly result from such solvation, stabilizes d_{yz} with respect to d_{xz} and reduces Δg_{xx} (Figure 4). Dichloromethane interacts very efficiently in this manner (Table V), reducing the intermediate g value from 2.079 to 2.053 and giving a distinctly rhombic appearance to the powder spectrum.[12a] The effect has been noticed before in the tendency of d^7 square-pyramidal metal carbonyls, notably $\{Fe(CO)_5^+\}$,[30b] to bond quite strongly with Kr. Such "solvation" results in a marked reduction in the in-plane g values of the uniaxial species.

Facile bending of the CO ligands within the equatorial plane may also explain the marked temperature dependence of the polycrystalline EPR spectrum (Supplementary Information); the extreme g value features broaden and approach each other with increasing temperature while the intermediate g features remain unaffected, at least initially. This behavior is an indication of motion, within the equatorial plane, which may be envisaged as involving a hopping of the symmetry axis of the square pyramid among the three equatorial bonds, C(1–3), of the host cation. Such motion would involve a trigonal-bipyramidal intermediate, isomerization to which our theoretical calculations (see below) suggest would be formally symmetry forbidden. However, the calculations also suggest that the energy difference between square-pyramidal and trigonal-bipyramidal isomers with mutually trans phosphines is only about 25 kJ mol^{-1} and that the activation energy for this process is about 40 kJ mol^{-1}. Furthermore, the observation that the (axial CO)–Fe(basal CO) bond angles, C(1)–Fe–C(2) and C(1)–Fe–C(3), differ by almost 5° (Table III) is consistent with a rather shallow potential well for the postulated bond angle deformation.

The potential minimum associated with Co–C(1) is evidently significantly lower than the alternatives, since only one configuration is observed. The exclusive choice of Co–C(1) for the symmetry axis of the square-pyramidal impurity center is a manifestation of the low symmetry of the host crystal; there is no true 3-fold axis, so that the three equatorial carbons are distinct in the crystal. However, the other minima will undoubtedly be close in energy and barriers beween them may be small; in-plane bending is presumably the least energetic pathway connecting the minima of the triple potential well. From the difference between g_{yy} and g_{zz}, we estimate that motion causing averaging in the spectrum has an effective frequency of $\cong$300 MHz at room temperature. A truly averaged spectrum for a uniaxial radical with a unique principal value equal to g_{xx} and perpendicular values equal to $(g_{yy} + g_{zz})/2$ was not observed; at temperatures approaching ambient, other motions evidently became important, resulting in a broad spectrum centered at the mean g value.

The ^{31}P hyperfine interactions are typical[30c] of phosphine ligands in transition-metal radicals; they are small and only slightly anisotropic. Within the limitations imposed by the small anisotropy (Table IV) and the line width, the hyperfine interaction matrices for the two ^{31}P nuclei were coparallel; they were nearly uniaxial with unique values directed within 4° of the host Co–P bonds. Resolving the principal values of $\mathbf{a}_{31}$ into isotropic and anisotropic contributions

$$\mathbf{a}_{31} = 53.9 + (7.3, -4.0, -3.3)\ \text{MHz} \qquad (2)$$

we note that the traceless matrix has diagonal components close

(31) Goodman, B. A.; Raynor, J. B. *Adv. Inorg. Chem. Radiochem.* **1970**, *13*, 135.
(32) McWeeney, R. *Couson's Valence*; Oxford University Press: Fair Lawn, NJ, 1979; Chapter 9.
(33) Cotton, F. A.; Wilkinson, G. *Advanced Inorganic Chemistry*, 5th ed.; Wiley & Sons: New York, 1988; p 57.
(34) Hoffmann, R. *J. Chem. Phys.* **1963**, *39*, 1397.

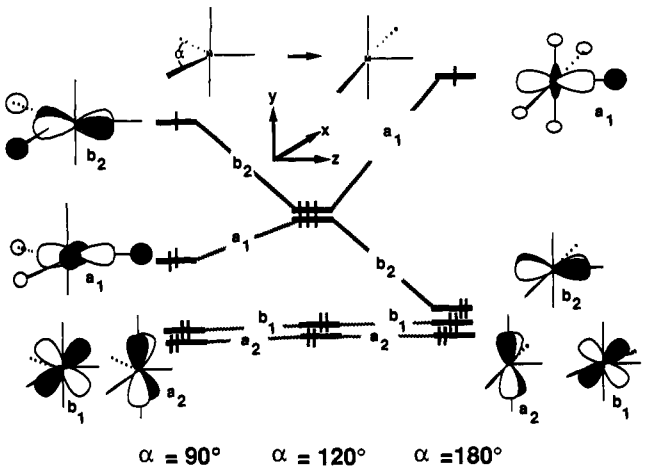

Figure 6. Orbital diagram for $\{Mn(CO)_5\}$ and $\{Fe(CO)_5^+\}$ correlating the upper occupied levels in the bipyramidal (left) and square-pyramidal (right) conformations.

to those expected for a point-dipolar interaction between an electron centered 2.28 Å (Fe–P bond length in the radical $\{Fe(CO)_3(PPh_3)_2^+\}$] from a ^{31}P nucleus

$$a_{dip} = (4.5, -2.7, -2.7)\ \text{Mhz} \qquad (3)$$

Moreover, the unique directions, i.e. along Fe–P, coincide. We conclude, therefore, that the dipole–dipole contribution dominates the anisotropic phosphorus hyperfine interaction and that phosphorus 3d direct contributions to the SOMO are less than 0.3%. We are furthermore able to say that the Fe–P directions must be close to those of Co–P in the host, i.e. P–Fe–P is almost linear.

Theoretical Considerations. Orbital level diagrams for $\{Mn(CO)_5\}$ and $\{Fe(CO)_5^+\}$ are given in Figure 6. The right-hand side of Figure 6 corresponds to a square-pyramidal geometry, **1a**, the center portion to a symmetric (trigonal) bipyramidal (D_{3h}) geometry, and the left-hand side to a bipyramidal, **1b**, geometry. The orbitals are classified according to C_{2v} symmetry. The two 17-electron complexes have in **1a** an $(a_2)^2(b_1)^2(b_2)^2a_1$ configuration of $^2A_1$ symmetry with a single electron residing in the d_{z^2}-based a_1 orbital.

1a **1b**

The optimized geometries for $\{Mn(CO)_5\}$ and $\{Fe(CO)_5^+\}$ of structure **1a** have been calculated, with the finding that the four basal CO ligands are in both cases bent slightly away from the apical ligand with C_{bas}–M–C_{ap} angles of 92–93°. On the other hand, reduction of the angle (α) between two trans ligands in the basal positions of **1a** will gradually lead to the bipyramidal structure, **1b**. We give on the left-hand side of Figure 6 an orbital level diagram for the bipyramidal case where α or **1b** is respectively 120° (trigonal bipyramidal) and 90° (pyramidal). It follows from Figure 6 that structure **1b** could have an $(a_2)^2(b_1)^2(b_2)^2a_1$ ground-state configuration of $^2A_1$ symmetry, just as **1a**. It might alternatively adopt an $(a_2)^2(b_1)^2(a_1)^2b_2$ ground-state configuration of $^2B_2$ symmetry. The $^2A_1$ state does not have a minimum for the bipyramidal structure, **1b**, but converges back to the square-pyramidal geometry, **1a**. However, the $^2B_2$ state adopts for both $\{Mn(CO)_5\}$ and $\{Fe(CO)_5^+\}$ a bipyramidal geometry in which α is 97–98°.

This distortion from the ideal trigonal geometry (α = 120°) stabilizes the fully occupied a_1 orbital (Figure 6) by nearly eliminating the antibonding interaction between the metal-based $d_{x^2-z^2}$ orbital and the σ orbitals on the two CO ligands that are bending back. The singly occupied b_2 orbital is at the same time raised in energy as the antibonding interaction between d_{xz} and the σ orbitals on the two bending CO ligands is increased (Figure 6). The total distortion from α = 120° to 97–98° is thus seen to be stabilizing. We note that the σ orbital on the unique equatorial ligand in structure **1b** has a strong antibonding interaction with $d_{x^2-y^2}$ on the metal in the fully occupied a_1 orbital (Figure 6). The corresponding M–CO bond is as a consequence elongated by 0.1 Å compared to the two other equatorial M–CO bonds. It follows from Figure 6 that a 17-electron complex with a trigonal-bipyramidal structure of α = 120° would distort to either a square-pyramidal geometry where $\alpha \approx 180°$ or a bipyramidal structure where $\alpha \approx 100°$. In either of the distortions, one pair of electrons is lowered in energy whereas the orbital holding the single electron is raised, the total effect thus being stabilization of the system. In contrast, similar distortions for an analogous 18-electron complex would be less favorable as one pair of electrons would now be raised as much or more in energy as the other is lowered. Thus the trigonal-bipyramidal structure is favored.

The two isomers **1a** and **1b** were found to be close in energy for both $\{Mn(CO)_5\}$ and $\{Fe(CO)_5^+\}$; structure **1a** is calculated to be 11 kJ mol^{-1} more stable than **1b** for $\{Mn(CO)_5\}$ whereas **1b** is 7 kJ mol^{-1} more stable than **1a** in the case of $\{Fe(CO)_5^+\}$. Thus the structures assumed may well be dependent on medium effects although, as mentioned above, only **1a** has been observed for these and similar species.

Figure 7 presents the energies of the $^2A_1$ and $^2B_2$ states for each of the two optimized geometries of $\{Mn(CO)_5\}$. For structure **1a**, the $^2B_2$ state is above $^2A_1$ by 174 kJ mol^{-1} whereas, for **1b**, $^2A_1$ is above $^2B_2$ by 102 kJ mol^{-1}. It follows from Figure 7 that the interconversion between the square-pyramidal isomer, **1a**, and the bipyramidal isomer, **1b**, is formally a symmetry-forbidden process; the energy of 60 kJ mol^{-1} at the crossing of the two lines correlating the $^2A_1$ and $^2B_2$ states in Figure 7 can be taken as a rough estimate of the energy barrier for the interconversion between **1a** and **1b**. Our findings are thus consistent in part with an earlier theoretical prediction of a square-pyramidal structure, based on extended Hückel calculations,[34] by Elian and Hoffmann.[9a] We also find, however, a second minimum corresponding to a bipyramidal structure, **1b**. The general study on metal carbonyl fragments by Elian and Hoffmann[9a] did not consider the structures of 17-electron $\{M(CO)_5\}$ complexes in detail, but simply concluded that $\{M(CO)_5\}$ is square pyramidal since the radical in this structure is of lower energy than $\{M(CO)_5\}$ in a trigonal-bipyramidal structure, **1b**, where α = 120°. A decrease of α from 120° was not considered.

We have similarly optimized structures **2a–c** from both $\{Mn(CO)_3(PH_3)_2\}$ and $\{Fe(CO)_3(PH_3)_2^+\}$, finding (Figures 8 and 9) that the three geometries are of quite similar energies for both species. The cis isomer, **2b**, was found to be the most stable for

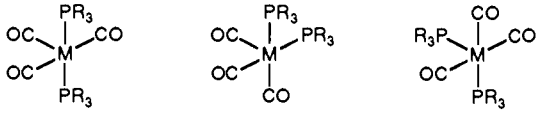

2a **2b** **2c**

$\{Mn(CO)_3(PH_3)_2\}$ whereas **2a** and **2c** are respectively 4 and 14 kJ mol^{-1} higher in energy. A similar situation was found for $\{Fe(CO)_3(PH_3)_2^+\}$, where **2b** again is the most stable isomer with **2a** and **2c** respectively 3 and 7 kJ mol^{-1} higher in energy. It is likely that steric factors in phosphines with bulkier substituents will favor the trans structure, **2a**, and indeed, molecular mechanics calculations on the three isomers suggest that forcing two PPh_3 ligands into mutually cis positions costs ≈50 kJ mol^{-1} relative to **2a**.[35]

In addition to **2a–c**, there are five possible bipyramidal isomers for $\{Mn(CO)_3(PH_3)_2\}$ and $\{Fe(CO)_3(PH_3)_2^+\}$. We have only considered the two, **2d** and **2e**, in which a pair of CO ligands is bent back in the equatorial plane since the other isomers, in which

(35) We have utilized PCModel on a Sun SPARCStation 1, from Serena Software, Bloomington, IN.

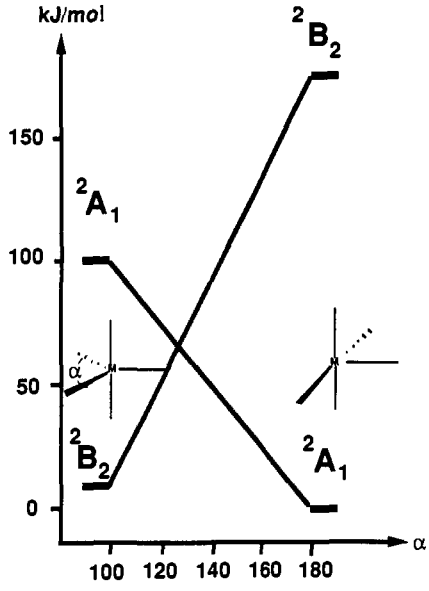

Figure 7. Diagram correlating the ground state and first excited state of $\{Mn(CO)_5\}$ in the bipyramidal conformation (left) and the square-pyramidal conformation (right).

one or two phosphine ligands are bent back, should be sterically more demanding, in particular for bulkier substituents.

The optimized bipyramidal structures are shown in Figures 8 and 9 for $\{Mn(CO)_3(PH_3)_2\}$ and $\{Fe(CO)_3(PH_3)_2^+\}$, respectively.

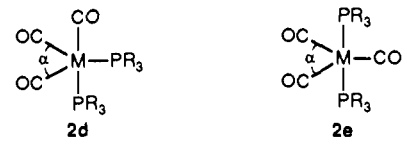

2d **2e**

We note that the bipyramidal structures are comparable in energy to the square-pyramidal geometries, with **2d** being somewhat (≈13 kJ mol^{-1}) more stable then **2e**. This situation might well change for bulkier phosphines, in which **2e**, with the PR_3 ligands trans, would be more favorable. The bisphosphine radicals with a bipyramidal geometry have the single electron in a d_{xz} orbital, just as do the pentacarbonyls (Figure 6). The interconversion between a square-pyramidal and a bipyramidal geometry can therefore be considered as for the pentacarbonyl analogues, and we estimate the activation barriers for the process **2a** → **2e** as 41 and 73 kJ mol^{-1} for $\{Fe(CO)_3(PH_3)_2^+\}$ and $\{Mn(CO)_3(PH_3)_2\}$, respectively.

Summary

We have shown by X-ray crystallography and single-crystal EPR spectroscopy that the cationic, iron-centered radical $\{Fe(CO)_3(PPh_3)_2^+\}$ assumes an essentially square-pyramidal geometry in the solid state and in solution. The EPR evidence is now quite unambiguous, the observed g factors being clearly those of a d_{z^2}, not a d_{xz} species. Furthermore, with the exception of $\{Mn(CO)_5\}$, the EPR spectrum of which has not been observed in the liquid state, the agreement between isotropic parameters and the averaged anisotropic parameters of all five-coordinated, 17-electron organometallic radicals investigated in this way shows that the square-pyramidal geometry is retained in the liquid state in all cases.

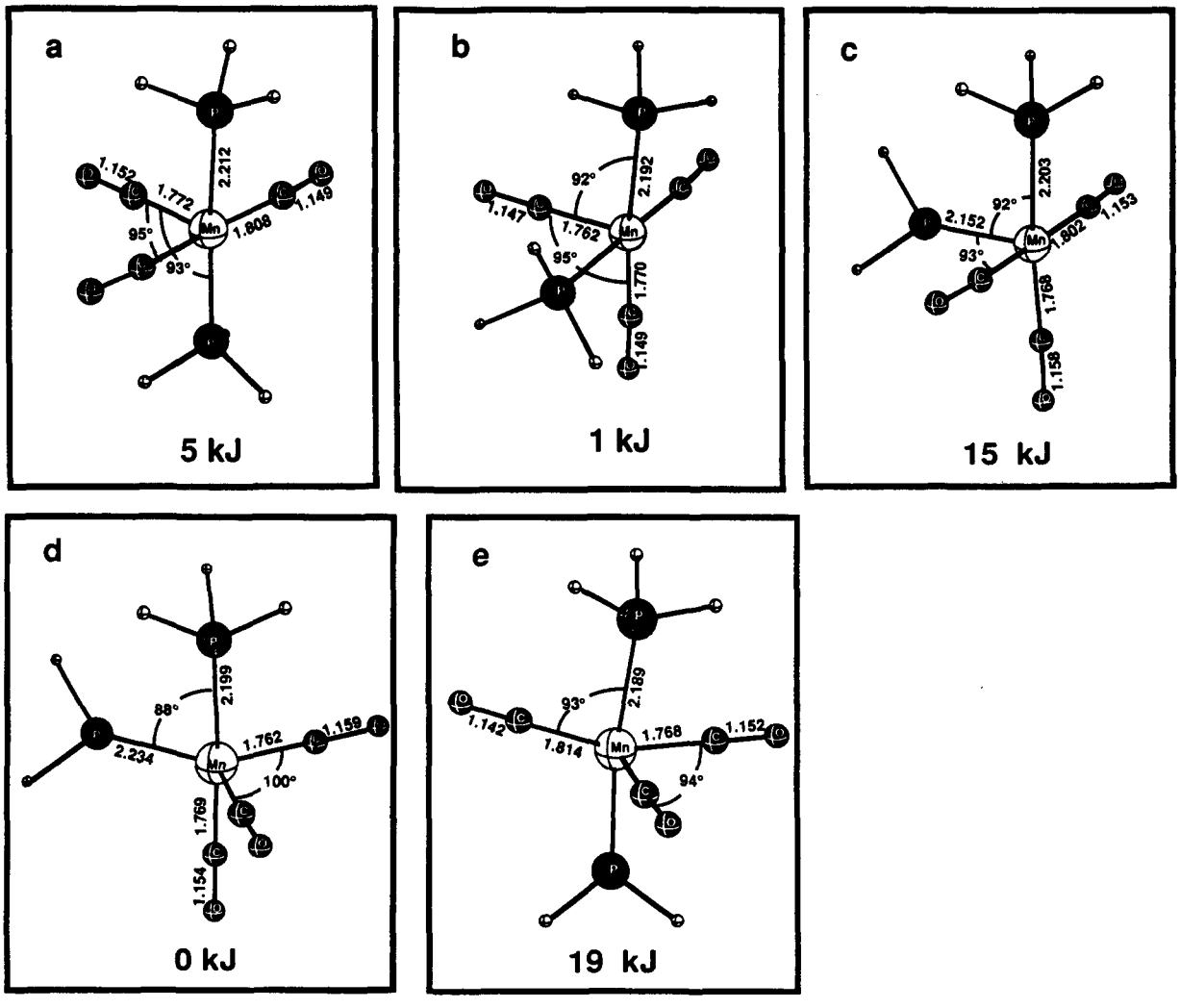

Figure 8. Optimized structures for $\{Mn(CO)_3(PH_3)_2\}$. All energies are with respect to the bipyramidal geometry of **1d** which has the lowest energy.

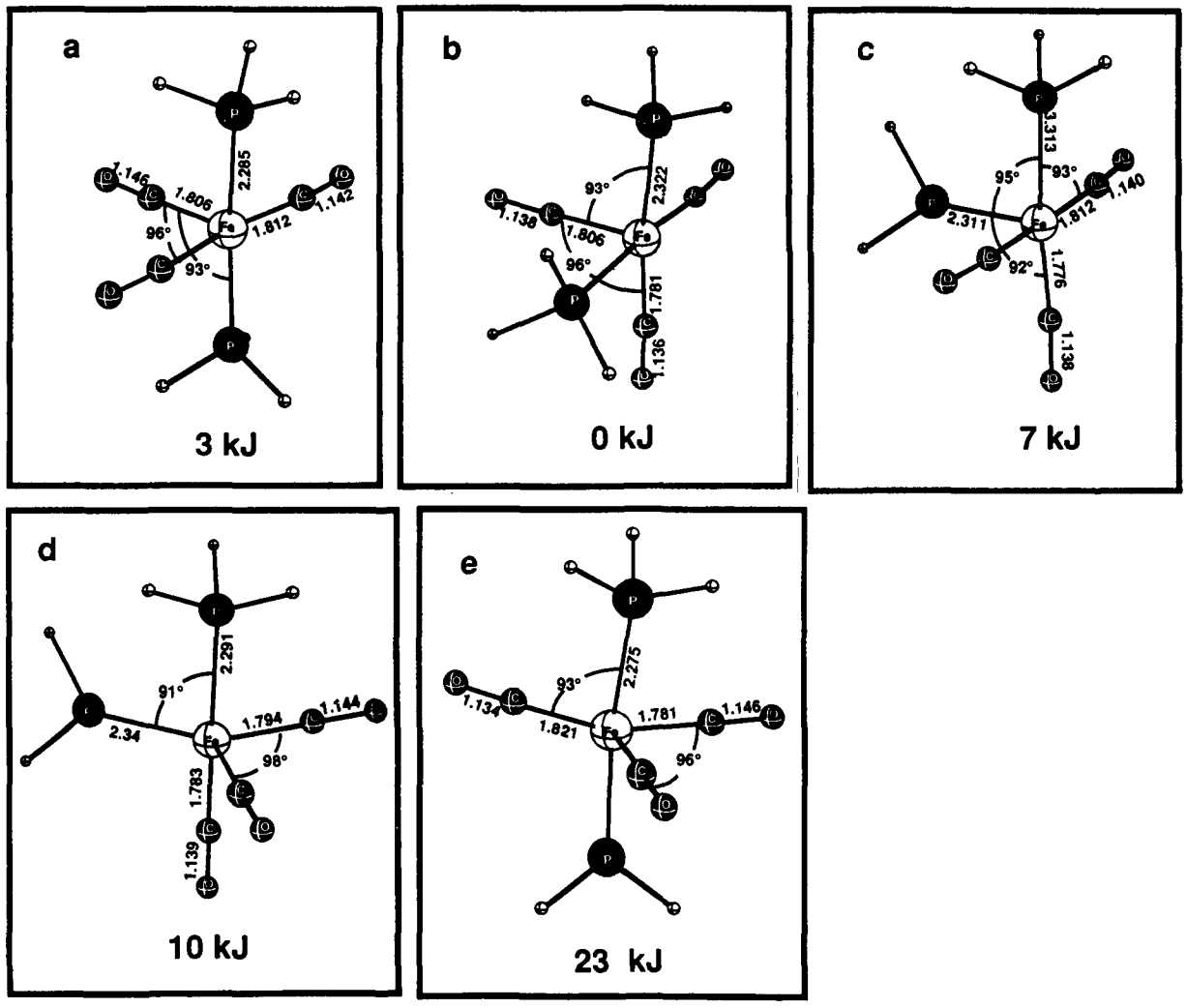

Figure 9. Optimized structures for $\{Fe(CO)_3(PH_3)_2\}$. All energies are with respect to the square-pyramidal geometry of **2b** which has the lowest energy.

Thus previous, apparently incongruous, reports[12] of well-resolved room temperature EPR spectra of this and similar species have been rationalized. Although we do not as yet have an explanation to offer for observation of only a single ν(CO) for solutions of $\{Fe(CO)_3(PPh_3)_2^+\}$ salts in dichloromethane,[12e] we confirm that a single, symmetric absorption in the dichloromethane solution of $[Fe(CO)_3(PPh_3)_2]PF_6$ is indeed observed, and that $\Delta\nu_{1/2}$ for the band (17 ± 3 cm^{-1}) is in fact significantly less than that of the corresponding band in the spectrum of $[Co(CO)_3(PPh_3)_2]PF_6$ (22 ± 3 cm^{-1}). Conceivably the species $\{Fe(CO)_3(PPh_3)_2^+\}$ is fluxional with respect to exchange for the carbonyl ligands; carbonyl site exchange which is rapid on the IR time scale is rare but does have precedent,[36] and we note from the EPR evidence discussed above that such exchange occurs in the solid state. However, we note that the IR spectrum of the very similar radical, $\{Re(CO)_3(PCy_3)_2\}$, also exhibits only a single ν(CO),[11] suggesting either that many species of this type may be fluxional on the IR time scale or that accidental degeneracy of the normal modes is common.

Our LCAO–HFS energy-optimized calculations for $\{Mn(CO)_5\}$, $\{Fe(CO)_5^+\}$, $\{Mn(CO)_3(PH_3)_2\}$, and $\{Fe(CO)_3(PH_3)_2^+\}$ indicate the existence in all cases of two nearly equienergetic isomers, a square-pyramidal structure with large metal d_{z^2} character in the SOMO and a bipyramidal structure with a d_{xz} SOMO. The pairs of isomers are separated by moderate energy barriers (50–75 kJ mol^{-1}), and thus the actual structures realized by the radicals by low temperatures may be influenced by the way in which they are generated and/or by subtle medium effects. The experimental data to date are unequivocally in favor of square-pyramidal structures for all.[5-11]

A particularly striking result of this investigation is the observation of retention of square-pyramidal geometry for the cation $\{Fe(CO)_3(PPh_3)_2^+\}$ upon substitution for the trigonal-bipyramidal host cation $\{Co(CO)_3(PPh_3)_2^+\}$. While it has been implied elsewhere that a host crystal lattice may force a dopant molecule to assume the structure of the host,[12e] it is clear that the pseudo-D_{3h} symmetry of the host cobalt cation is completely ineffective in forcing the dopant cation to adopt a similar structure.

Acknowledgment. We are indebted to the Natural Science and Engineering Research Council of Canada for operating grants to S.F., M.C.B., and T.Z. and for a graduate scholarship to J.H.M. We also thank Professors R. D. Heyding and S. F. A. Kettle for experimental assistance or helpful discussions.

Registry No. $[Co(CO)_3(PPh_3)_2]PF_6 \cdot CH_2Cl_2$, 137003-34-0; $[Fe(CO)_3(PPh_3)_2]PF_6 \cdot {}^1/_2CH_2Cl_2$, 137119-44-9; $[Co(CO)_3(PPh_3)_2]PF_6$, 137003-33-9; $[Fe(CO)_3(PPh_3)_2]PF_6$, 137119-43-8; $Fe(CO)_3(PPh_3)_2^+$, 137038-33-6; $Mn(CO)_5$, 71564-17-5; $Fe(CO)_5^+$, 59699-78-4; $Mn(CO)_3(PH_3)_2$, 137003-35-1; $Fe(CO)_3(Ph_3)_2$, 137038-34-7.

Supplementary Material Available: Complete tables of positional and thermal parameters and figures showing (Figure 1) g^2 values as a function of angle, (Figure 2) the powder EPR spectrum at 77 K, (Figure 3) temperature dependence of the powder EPR spectrum, and (Figure 4) EPR spectrum in CH_2Cl_2 at 77 K (14 pages). Ordering information is given on any current masthead page.

(36) (a) Grevels, F.-W.; Jacke, J.; Klotzbücher, W. E.; Krüger, C.; Seevogel, K.; Tsay, Y.-H. *Angew. Chem., Int. Ed. Engl.* **1987**, *26*, 885. (b) Grevels, F.-W.; Jacke, J.; Seevogel, K. *J. Mol. Struct.* **1988**, *174*, 107.